Atmospheric Environment 318 (2024) 120281

Contents lists available at ScienceDirect

Atmospheric Environment

journal homepage: www.elsevier.com/locate/atmosenv

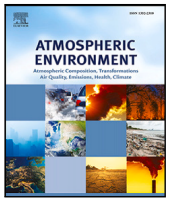

# Assessment of environmental consequences of hostilities: Tropospheric $NO_2$ vertical column amounts in the atmosphere over Ukraine in 2019–2022

Liudmyla Malytska [a,b,*], Annette Ladstätter-Weißenmayer [a], Evgenia Galytska [a,c], John P. Burrows [a]

[a] Institute of Environmental Physics, University of Bremen, Otto-Hahn-Allee 1, Bremen, 28359, Germany
[b] Ukrainian Hydrometeorological Institute, 37 Nauky Ave, Kyiv, 03028, Ukraine
[c] Deutsches Zentrum für Luft- und Raumfahrt (DLR), Institut für Physik der Atmosphäre, Oberpfaffenhofen, Germany

## HIGHLIGHTS

- The 2022 Russia-Ukraine conflict harmed the environment, impacting air pollution.
- Hostilities reduced industrial $NO_2$ emissions but intensified fires in Ukraine.
- Fires in Chornobyl raised $NO_2$ to pre-conflict levels, holding trans-border impact.

## ARTICLE INFO

Dataset link: https://dataspace.copernicus.eu/, https://earthdata.nasa.gov/firms, https://ads.atmosphere.copernicus.eu/cdsapp#!/dataset/cams-global-fire-emissions-gfas, https://www.ecmwf.int/en/forecasts/datasets/reanalysis-datasets/era5, https://www.wetter3.de/archiv_dwd_en.html, https://www.ready.noaa.gov/HYSPLIT.php

*Keywords:*
Tropospheric $NO_2$
Effects of hostilities
Atmospheric pollution processes
HYSPLIT

## ABSTRACT

The invasion of Ukraine by Russia started on 24 February 2022. The armed conflict has been accompanied by atmospheric and soil pollution, deterioration of fresh water, and the creation of irreversible changes in ecosystems. This study focuses on the effects of hostilities on tropospheric pollution. It comprises an analysis of the spatiotemporal tropospheric $NO_2$ distribution over Ukraine for the period 24 February–06 May 2022 from the TROPOMI satellite instrument. We compared the tropospheric columns of $NO_2$ during the first 72 days of hostilities to values for three pre-hostilities periods: pre-COVID-19, COVID-19 lockdown and adaptive lockdown, to differentiate the effects of COVID-19 restrictions and active hostilities on $NO_2$ emissions over Ukraine. We used VIIRS satellite instrument data to study fire distribution and its intensity and confirm their influence on the tropospheric $NO_2$ level as well as investigate the extent to which the hostilities affect fire frequency. Additionally, we analyzed the transborder and regional air mass transport from the origin of the fires using the HYSPLIT model version 5.2 and supported it with the analysis of near-surface weather charts.

The results indicate that hostilities in Ukraine have a direct impact on atmospheric pollution processes. Hostilities resulted in an unprecedented reduction in economic activity, comparable to the COVID-19 pandemic lockdown, and correspondingly, reduced $NO_2$ emission in industrial areas, which equals about 2–4 $\times 10^{15}$ molec $cm^{-2}$, whereas the $NO_2$ concentration locally increased in the areas of conflict. While we detected temporal $NO_2$ decline, hostilities negatively affected air quality in Ukraine due to the significant increase in frequency and intensity of fires, especially in conflict-related areas. Air pollution, in the case of one-off strikes, tends to be a short-term phenomenon, but frequent attacks on large military targets cause atmospheric consequences on local as well as on regional levels. During the first 72 days of hostilities, we linked bursts of fires with significant air pollution over northern (Kyiv and Zhytomyr regions), southern (Odesa, Kherson regions), and eastern (Donetsk region) parts of Ukraine. Based on the TROPOMI and VIIRS data, it was figured out that forest fires over the Kyiv region and Chornobyl Exclusion Zone, driven by military actions on 19–23 March 2022, caused the $NO_2$ content increase from 3 to 17.5 $\times 10^{15}$ molec $cm^{-2}$, which is comparable to the most polluted Ukrainian industrial cities during the pre-hostilities period. As a result, the most affected territories were located within 50 km of active fires, but air quality deterioration was observed at a distance of about 200 km downwind. HYSPLIT version 5.2 forward trajectories simulation showed that a smoke-particle-included air mass, related to the fires in the Chornobyl Exclusion Zone was extended to Romania, Serbia, Kosovo, and Albania towards the Mediterranean Sea at the height of 530 m. At 1.5–3 km altitudes, the air parcels were transported to Poland and countries of the Baltic region. At 3 km height, the air mass reached the Russian Federation in 72 h.

* Corresponding author at: Ukrainian Hydrometeorological Institute, 37 Nauky Ave, Kyiv, 03028, Ukraine.
*E-mail address:* lmalytska@iup.physik.uni-bremen.de (L. Malytska).

https://doi.org/10.1016/j.atmosenv.2023.120281
Received 20 September 2023; Received in revised form 4 December 2023; Accepted 5 December 2023
Available online 9 December 2023

## 1. Introduction

After the occupation of parts of Ukraine in 2014, an invasion of Ukraine by Russia began on 24 February 2022. In addition to the loss of life and property, another result of these hostilities is the change in environmental conditions in Ukraine and surrounding regions. Examples of this are changes in atmospheric pollution, reduced quality of fresh water, and both reversible and irreversible changes to ecosystems and thus ecosystem services. The focus of this study addresses changes in tropospheric pollutants. Specifically oxides of nitrogen $NO_x$ (i.e. $\Sigma$ nitric oxide (NO) and nitrogen dioxide ($NO_2$) are investigated by using the tropospheric column of $NO_2$ as a surrogate. During the period of hostilities, the tropospheric column amount of $NO_2$ is modified by the following factors. Firstly, it is a changing population and its distribution, as a result of refugees leaving the region, and the mobilization of two armies. This alters the $NO_x$ emitted by domestic heating, industry, agriculture, and transport. Secondly, air pollutants are released by the attacks on chemical and metallurgical plants. In addition, mines that have become targets of attacks also can become a source of pollution, leading to further environmental impacts. All of the above results of the war have negative impacts on the health of the population, sustainable development, and food security, especially in the eastern and southern regions of Ukraine where most of the fighting takes place. However, the results of the war influenced not only the eastern and southern parts but also the entire territory of Ukraine. Within the first eight months of hostilities, the State Environmental Inspectorate of Ukraine recorded that 680,618 tons of petroleum products were burned during the shelling and 23,286 hectares of forest were on fire (see https://new.dei.gov.ua/posts/2408, last access: 05.11.2022). As a result of the bombings and rocket attacks over the Chornobyl Exclusion Zone and in the reed thickets in river floodplains of the Azov-Black Sea region, namely in the Danube biosphere reserve and Kinburn spit regional landscape park, large-scale fires (10,000 hectares) were observed. By June 2022, the State Environmental Inspectorate of Ukraine had reported at least seven confirmed incidents with the release of toxic industrial chemicals caused by military activities (see https://www.dei.gov.ua/posts/2226, last access: 18.01.2023). A number of studies have previously shown that these large and frequent fires are significant sources of increased abundance of aerosols and other pollutants (see for example, Barnaba et al., 2011; Griffin et al., 2021; Fan et al., 2023), with the focus on Eastern and Central Europe (Bovchaliuk et al., 2013; Bondur et al., 2019), and in particular on Ukraine (Galytska et al., 2018; Savenets et al., 2020; Zhang et al., 2022). The increasing intensity and severity of fires are expected to reduce air quality.

The hostilities in eastern Ukraine, officially known as the Anti-Terrorist Operation (ATO), which began in 2014, as reported by Vasyliuk et al. (2015) caused and continue to cause changes in the environment such as damage to rural areas, increasing fire frequency, disruptions of industry in the region. The occupation and attempted annexation of Crimea, as well as hostilities in the ATO zone, were named as critical factors in the sharp decline of total greenhouse gas emissions in 2014. This is attributed to the considerable reduction in industrial production and, as a consequence, reduction in energy consumption (Lyashenko et al., 2022). Hence, military actions, which halt industrial activities lead to a temporary reduction of pollution in eastern Ukraine.

Previous scientific publications have identified a range of effects of past armed conflicts and wars on atmospheric pollution and air quality. For example, the Kuwait war in February 1991 resulted in fires from the destruction of oil wells. Hobbs and Radke (1992) used observations from the airborne measurement campaigns to investigate the optical properties of the smoke, its chemical composition, the amounts, and rates of trace gas emissions, as well as the potential effects of this pollution on air quality, weather, and climate. They showed that smoke significantly affected air quality in the Persian Gulf, however, the global impact was insignificant. This is explained as follows. The particle emissions were less than expected, and the smoke was not as black as expected. In addition, the plume was never observed to rise above 6 km height, well below the base of the stratosphere in this region (i.e. around 13 km), and as a result, the smoke had a short atmospheric residence time. At the same time, a smoke-particle-induced increase of aerosol light absorption at the Mauna Loa Observatory, Hawaii was seen, which could be traced back to oil burning in Kuwait in February 1991 Bodhaine et al. (1992) and Lowenthal et al. (1992). Using the large-scale backward trajectories at 500 hPa the authors demonstrated direct transport paths from China and Kuwait to Hawaii, which indicates that the pollution incident was based on long-range transport in the free troposphere and had a significant transboundary impact.

Experience from the Kosovo war, which occurred from February 1998 to June 1999, also indicates that frequent attacks on major industrial plants, such as fuel storage tanks, machine industry, food-processing plants, heating plants, water-treatment plants, and the electric power grid including transformers, caused many industrial accidents and fires. These resulted in the release of various air pollutants such as Semi-Volatile Organic compounds (SVOs), in particular, organic phthalates, which were investigated by Melas et al. (2000) and persistent organic pollutants (POPs), which were studied by Vukmirović et al. (2001). These studies describe the consequences and subsequent transboundary transport of pollutants from the burning or damaging of industrial sites and other military targets. The authors linked these military conflicts to significant air pollution episodes. The attacks on the industry were in Northern Serbia and in the vicinity of Belgrade and polluted air masses were transported to Bulgaria, Romania, Ukraine, Moldova, and the Black Sea region. The distribution of the transboundary pollution was investigated by calculating backward trajectories, using the Hybrid Single-Particle Lagrangian Integrated Trajectory model version 4 (HYSPLIT-4, Melas et al., 2000; Vukmirović et al., 2001).

A first attempt to statistically estimate the impact of hostilities on $NO_x$ and Carbon Dioxide ($CO_2$) emissions per capita, as well as on the rate of change in a forested area, and a composite indicator of environmental stress reduction for a large-N sample was published by Reuveny et al. (2010). The study showed that military conflicts reduce the $CO_2$ emissions, regardless of the location of the conflict at home or abroad ("home" and "abroad" terminology defined by Reuveny et al., 2010), but the impact is weaker in less developed countries (LDCs) than in developed countries (DCs). This result is attributed to the generally non-industrialized nature of economies in LDCs. For $NO_x$, hostilities at home reduce emissions for the LDCs and increase them for the DCs, but conflict abroad increases $NO_x$ emissions for both the DCs and LDCs. The authors explained the varying impacts of hostilities on $NO_x$ emissions in LDCs and DCs as follows. Conflicts in DCs were largely non-destructive at home and highly mechanized, which could lead to increased emissions. Conversely, conflicts in LDCs typically involve the destruction of infrastructure such as plants, roads, and vehicles, which may result in reduced emissions. That is in agreement with the preliminary estimation of spatial and temporal responses of atmospheric composition to the Russia–Ukraine armed conflict in 2022, shown in Zhang et al. (2023), which investigated, not only in Ukraine but also Russian cities bordering Ukraine. They showed that $NO_2$ concentrations in most Ukrainian cities significantly decreased at the beginning of the war (by 10.7–27.3%), while in Russian cities outside the northern border $NO_2$ concentrations dramatically increased (by 31.7–77.0%). Another study focusing on the manifestations of the Russian–Ukrainian war across Central-East Europe (Wieczorek, 2023), found that $NO_2$ levels in Ukraine exhibited a dual trend, with significant drops of 33% observed in the Kyiv region, while a slight increase of 5% was observed in the Black Sea regions between 2021 and 2022.

Some preliminary conclusions about the environmental impacts of the military conflict in Ukraine are presented in the recent report by the United Nations Environment Programme (UNEP, 2022). The

report lists the damage, caused to the environment in Ukraine during the first seven months of hostilities, divided into six key areas: chemical industries and chemicals associated with armed conflict, fuel and related infrastructure, waste and waste infrastructure, urban and critical infrastructure, and damage to agriculture and to nature, that are often impacted by armed conflicts. The analysis indicates that the military action in Ukraine compounded pre-existing environmental issues, including air and water pollution, deforestation, and waste management. Additionally, it introduced new challenges like decreased agricultural productivity due to physical damage from military maneuvers and explosives, soil contamination from a large set of pollutants, loss of agricultural land from explosive remnants, such as unexploded ordnance or land mines, and destruction of irrigation infrastructure. However, UNEP (2022) report only briefly discussed the consequences (like incidents of the release of toxic industrial chemicals) of the hostilities on air pollution in Ukraine. Therefore, previous studies suggest that the consequences of hostilities in different areas of the world have an impact on atmospheric pollution. Specifically, there are often temporary reductions of $NO_2$ emissions resulting from lower economic activity but also increases due to an increased incidence of fires.

In this study, we focus on an analysis of the tropospheric $NO_2$ column amount retrieved from the Sentinel 5 Precursor (S5P) TROpopsheric Ozone Monitoring Instrument (TROPOMI) due to military conflict in Ukraine. $NO_2$ is an important short-lived and toxic tropospheric pollutant in its own right and a precursor of short-lived climate pollutants (SLCP) such as ozone ($O_3$) (Manisalidis et al., 2020). $NO_x$ is emitted to the troposphere by both naturally occurring processes (e.g. wildfires, lighting, and the biogenic degradation of natural sources of ammonium nitrate ($NH_4NO_3$)) and human activity (biomass burning, and fossil fuel combustion, which is used for domestic heating, industrial processes and to provide power for motor vehicles, shipping and aircraft, and the biogenic degradation of man-made fertilizers (i.e. $NH_4NO_3$). In the troposphere, $NO_x$ comprises NO, which reacts rapidly with $O_3$ to produce $NO_2$. $NO_2$ is then photolyzed to NO and an O atom, which then reacts with molecular oxygen $O_2$ in a termolecular reaction to reform $O_3$. As a result, NO, $NO_2$ and $O_3$ are in the Leighton photostationary state. However, in the presence of sufficient $NO_x$ and carbon monoxide (CO) or hydrocarbons, a chain reaction producing $O_3$ ensues (Fishman and Crutzen, 1978)

We have selected to study $NO_2$ tropospheric vertical column amount (VCD) distributions during 2019, 2020 and 2021, with a particular emphasis on comparing periods before and during hostilities. This analysis also includes the period of lockdown, where measures were introduced to control the spread of coronavirus (COVID-19), which reduced traffic and thus $NO_2$ emissions. In this study, we analyze the effects on $NO_2$ emissions that occurred during the COVID-19 lockdown and the hostilities, which have not been done before. In contrast to the works of Zhang et al. (2023) and Wieczorek (2023), we analyze the influence of fires and weather conditions on pollution incidents during hostilities. We associate pollution incidents with fires during hostilities by observations of the tropospheric $NO_2$ VCD increase taking place during fires caused by the conflict. In addition, we investigate the transport pathways of $NO_2$ using the HYSPLIT model version 5.2. We calculated trajectories of air pollution from the largest fire event caused by the conflict within the Kyiv region and Chornobyl Exclusion Zone in the lowest 3 km layer of the troposphere.

## 2. Data and methods

### 2.1. TROPOMI data for $NO_2$ tropospheric vertical column

Since some of the ground-based measurements in Ukraine are no longer under the control of the Government of Ukraine after the occupation of part of Ukraine by Russia in 2014 (Savenets, 2021), we have opted to utilize remote sensing as the sole feasible method for assessing the spatiotemporal variability of $NO_2$ across the entire territory. The TROPOMI instrument flies onboard the S5P satellite, which was launched on 13 October 2017. S5P flies in a sun-synchronous orbit having an equator crossing time of 09:30 in a descending node. S5P makes measurements of Ukraine between 12:00 Eastern European Summer Time (EEST) and 14:00 EEST (see e.g. Savenets et al., 2022). TROPOMI is a nadir-viewing hyperspectral spectrometer that builds on the heritage of SCIAMACHY (Burrows et al., 1995) and GOME (Burrows et al., 1999) and measures the backscattered UV–visible (270–500 nm), the near-infrared (NIR, 710–770 nm), and the shortwave infrared (2314–2382 nm) wavelength ranges upwelling form the top of the atmosphere and the extraterrestrial solar irradiance. Mathematical inversion of these measurements yields daily global coverage on total columns of trace gases such as $O_3$, $NO_2$, CO, $SO_2$ (Sulfur Dioxide), $CH_4$ (Methane) and HCHO (Formaldehyde) and CHOCHO (Glyoxal) (Veefkind et al., 2012; van Geffen et al., 2020; Alvarado et al., 2020).

TROPOMI tropospheric $NO_2$ VCD, used in this study, are derived from the measurements of the UV–NIR spectrometer in the wavelength range 400–465 nm (van Geffen et al., 2020). For the TROPOMI tropospheric $NO_2$ retrieval the Dutch Ozone Monitoring Instrument (OMI) $NO_2$ (DOMINO) approach that was successfully applied for the OMI $NO_2$ retrieval (van Geffen et al., 2020), is used. DOMINO is based on a three-step approach. The first step is to obtain the $NO_2$ slant column density (SCD), using the Differential Optical Absorption Spectroscopy (DOAS) method, which determines the total amount of $NO_2$ in the effective light path from the sun through the atmosphere to the satellite. The second step is to separate the stratospheric and tropospheric SCDs of the total SCD, applying the $NO_2$ vertical profile information from a chemistry transport model and data assimilation (CTM/DA) system. And the third step is to convert these SCDs into $NO_2$ vertical stratospheric and tropospheric column densities by applying appropriate air-mass factors (AMFs, van Geffen et al., 2020; Eskes et al., 2022). To analyze the spatiotemporal distribution of $NO_2$ vertical tropospheric columns over Ukraine, we used TROPOMI Level 2 $NO_2$ data products with the daily temporal resolution and spatial resolution of 5.5 km along the satellite flight direction and 3.5 km in the perpendicular direction at nadir. We used reprocessed (S5P-PAL) and offline-mode (S5P-OFFL) data of version V02.03.01, freely available from the S5P-PAL data portaland Copernicus Data Space Ecosystem (https://dataspace.copernicus.eu/) for a time period of four years 2019–2022. According to Fehr (2016), specified random uncertainty of a single TROPOMI tropospheric $NO_2$ VCD measurement should be within 25%–50% accuracy, with a precision of $0.7 \times 10^{15}$ molec $cm^{-2}$. In their study, Tack et al. (2021) determined the level of uncertainty for TROPOMI Level 2 tropospheric $NO_2$ data of version OFFL V01.03.01, and reported it is $5.6 \pm 0.4 \times 10^{14}$ molec $cm^{-2}$. The TROPOMI tropospheric $NO_2$ VCDs version V02.03.01 exhibits an improvement of negative bias from −32% to −23% compared to the previous versions, due to modifications in the treatment of surface albedo and the implementation of the FRESCO cloud retrieval upgrade (Lange et al., 2022b). According to Eskes et al. (2021), S5P-PAL and S5P-OFFL products are in good agreement (within 5%–10%), have a seamless connection, and could be used for trend studies, as they are based on a one processor version. We analyze the tropospheric amount of the total $NO_2$ VCD, defined as the vertically integrated number of molecules per unit area between the surface and the tropopause (Lange et al., 2022a). As recommended by Eskes et al. (2021), we set a quality threshold of 0.75 to exclude regimental measurements, associated with cloud-covered scenes (cloud radiance fraction >0.5), part of the scenes covered by snow/ice, and problematic retrievals, from the analysis.

### 2.2. Selected periods for the $NO_2$ analysis

Traffic and economic activity in Ukraine in 2019–2022 were influenced by measures implemented to reduce the spread of the impact of COVID-19 and then later the hostilities following the Russian invasion of Ukraine. From 12 March 2020, the Ukrainian government-enforced

COVID-19 lockdown measures, which restricted mobility, have started. Lockdown measures have included the complete closure of international borders, airports, educational institutions, non-critical businesses and restricted citizen mobility. Substantial restrictions continued for 72 days until 22 May 2020. Thereafter much of the mobility was restored but restrictions were kept for entertainment and service spheres. Since COVID-19 restrictions in Ukraine were changing over time, simple averaging of TROPOMI $NO_2$ data during 2019–2022 smooths over the specific lockdown effects and does not represent the typical values of $NO_2$ tropospheric VCD at the time. For that reason, in the analysis of $NO_2$ tropospheric VCD observed in Ukraine, we define and distinguish four periods: "pre-COVID-19" (31.12.2019-11.03.2020) before all implemented strict restrictions associated with COVID-19, "COVID-19 lockdown" (12.03.2020-22.05.2020) associated with strict restrictions of economic and transport activity, "adaptive lockdown" (14.12.2021–23.02.2022), which covers the period of limited restrictions for business, and "hostilities" (24.02.2022–06.05.2022) associated with the beginning of the invasion of Ukraine by the Russian Federation armed forces. As strict COVID-19 restrictions were maintained for 72 days, to be consistent in the analysis, all defined periods have also a duration of 72 days. In this study, we consider the pre-COVID-19 period as being representative of the emissions of $NO_x$ and thus the $NO_2$ tropospheric VCD prior to the large impacts of COVID-19 lockdown, adaptive lockdown, and hostility periods. We often refer to the three following periods "pre-COVID-19", "COVID-19 lockdown", and "adaptive lockdown" as the "pre-hostilities" period. An assessment of the impact of hostilities on $NO_2$ content in Ukraine was accomplished by the comparison of the mean $NO_2$ tropospheric VCD for the periods before and during hostilities. Although $NO_x$ emissions and the removal of $NO_x$ are strongly dependent on the sources, sinks, solar insolation, which initiates the photochemical removal of $NO_x$, and wet and dry deposition, are very dependent on the conditions in a given period, averaging over 72 days smooths to some extent the $NO_2$ behavior. Nevertheless, we consider this to be a reasonable approach, to identify the large changes in $NO_x$ caused by the restrictions on movement during the pandemic and the impact of the hostilities following the invasion of Ukraine in 2022.

### 2.3. VIIRS data for the distribution of fires

The Visible Infrared Imaging Radiometer Suite (VIIRS) instrument on board the Suomi National Polar-orbiting Partnership (Suomi NPP) satellite is a joint project of the National Aeronautics and Space Administration (NASA) and the National Oceanic and Atmospheric Administration (NOAA, Schroeder et al., 2014). From the day it was fully commissioned on 19 January 2012, the VIIRS has provided unique operational environmental data products from the mathematical inversion of its 22 imaging and radiometric bands, which extend from 412 nm to 12 μm at two spatial resolutions. As follows the I-bands are of high-resolution (375 m), and M-bands are of moderate-resolution (750 m). This enables an extensive set of data products to be generated (i.e. 23 environmental data records) such as cloud data products (VIIRS Atmosphere L2 Cloud Mask Product), sea surface temperature, ocean color, polar wind, vegetation fraction, aerosol, fire, snow and ice, and vegetation (Cao et al., 2014). VIIRS also hosts a unique panchromatic Day/Night band, which is ultra-sensitive in low-light conditions. Both daytime and nighttime fires are identified. VIIRS observes the entire Earth's surface twice each day. It passes over the territory of Ukraine during the night between 02:33 and 03:47 EEST and during the day from 12:43 to 14:25 EEST (see e.g. Oreshchenko et al., 2020). The temporal separation between VIIRS and TROPOMI data products is less than 5 min, both having an equator crossing time near 13:30 local solar time. This formation flying enables synergistic data products to be exploited for scientific research.

To indicate the location of fires and their strength, we used VIIRS 375 m Near Real-Time files: (VNP14IMGTDL) VIIRS Active Fire and Thermal Anomalies product from S-NPP distributed by via NASA FIRMS (https://earthdata.nasa.gov/firms). The product has a retrieved pixel size of 375 $m^2$ viewed in nadir. The fire detection algorithm is described in Schroeder and Giglio (2018). These VIIRS data products provide knowledge about fire location, time, and burning characteristics like Fire Radiative Power (FRP). The latter is a measure of the energy, emitted by fire (i.e. the total fire intensity minus the power dissipated through convection and conduction) over its entire area and is used as an indicator of fire intensity. FRP has units of MWatts (MW). Each VIIRS fire pixel is also accompanied by a confidence value, which expresses in % the probability of a fire being within a ground scene or pixel. Confidence values defined as "low", "nominal", and "high" are matched to the confidence intervals of 0%–29%, 30%–79%, and 80%–100% respectively. Fire pixels with "low" or "nominal" confidence values were filtered out and not used, to avoid pixels contaminated by sun glint and small relative temperature anomalies (i.e. $\Delta T < 15$ K).

In this study, we used daily data on fire location and FRP from 2021–2022. First, we focus on the period January–September 2021 to evaluate the distribution of fires before the beginning of the invasion of Russian troops in 2022. Then, we analyze the same months but during the year 2022, which includes the first seven months of hostilities. This analysis enables the influence of the hostilities on the occurrence and distribution of fires in Ukraine to be assessed. Finally, we analyze the daily variations of fires during the period of hostilities, as defined in Section 2.2. In addition, we identify fire episodes caused by the hostilities and associated with high levels of air pollution and undertake a case study for the largest of these fires.

To connect specific events during the hostilities to fire and pollution episodes, we used the interactive map provided by "Liveuamap" (https://liveuamap.com/, last access: 13.02.2023). This map identifies events related to the hostility and illustrates areas of control, relying primarily on social media geotags to determine location. The Centre for Humanitarian Dialogue (HD) and the United Nations Department for Political and Peacebuilding Affairs (UN DPPA) Middle East Division applied this tool in Syria to monitor the implementation of the ceasefire and to assess the feasibility of humanitarian corridors as well as to contribute to ensuring the security of its staff when traveling to Syria (UNDPPA and HD, 2019).

### 2.4. GFAS data for the flux of $NO_x$ originating from fires and biomass burning

The Global Fire Assimilation System (GFAS) is the global fire emission inventory provided by the Copernicus Atmosphere Monitoring Service (CAMS) (https://ads.atmosphere.copernicus.eu). It serves as a widely utilized and authoritative tool for quantifying and comprehending biomass burning emissions both on a global and local scale (Jin et al., 2023; Di Giuseppe et al., 2018). GFAS integrates data from FRP observations obtained from the Moderate Resolution Imaging Spectrometer (MODIS) instruments on NASA's Terra and Aqua satellites. The GFAS data provides gridded information on FRP, dry matter burnt, and emissions from biomass burning for 40 gas-phase and aerosol species. It is globally accessible on a regular latitude–longitude grid with a horizontal resolution of 0.1°, covering the period from 2003 to the present. It also provides information about injection heights based on satellite-observed FRP and the European Centre for Medium-Range Weather Forecasts (ECMWF) weather forecast (Rémy et al., 2017). The system corrects for observational gaps caused by factors such as cloud cover and filters out spurious FRP readings associated with non-biomass burning sources, including volcanoes and industrial activities. GFAS consistently provides reliable estimates for the magnitude and timing of fire emissions, with uncertainties generally around 30% and slightly higher for exotic species (Andela et al., 2013). In this study, we used daily GFAS data (version 1.2) on the wildfire flux of nitrogen oxides and the altitude of plume top from March 2023.

### 2.5. Transport of air masses and meteorological data

To analyze the regional transport of pollutants, we used the model output of the trajectory analysis model HYSPLIT version 5.2 developed by NOAA Air Resources Laboratory (Stein et al., 2015). The HYSPLIT version 5.2 combines (i) a moving frame of reference that follows air parcels as they move from their initial location to simulate advection, diffusion, and deposition (Lagrangian approach) and (ii) a fixed three-dimensional grid as a frame of reference to compute the pollutant air concentrations (Eulerian approach).

To study the $NO_2$ transport from the largest fires and to assess its transboundary impact, we computed forward trajectories of the air masses at different heights (mid-boundary layer height, 1.5 km, and 3 km) for dates of the maximum measured $NO_2$ at each point. The starting "mid-boundary layer height" is defined as one-half the mixed layer height and is taken from the Global Forecast System (GFS) meteorological data set. The atmospheric boundary layer is a turbulent layer that is directly affected by the underlying Earth's surface and reacts to the influence of the surface during a short period of time (within approximately an hour). The mixed layer height is important for understanding the structure of the lower troposphere, as it determines the volume available for pollutant dispersion (Dang et al., 2019). The 1.5 km height was chosen as an approximation unaffected by the orographic features of the surface and corresponds to the isobaric surface of 850 hPa. The 3 km height lies on the isobaric surface of 700 hPa and characterizes the distribution of air flows in the troposphere. We also chose the lower 3 km layer based on the previous analysis, which showed that the particles (for instance, aerosols) are concentrated in the lowest 3–5 km tropospheric layer (e.g. Fig. 9 in Galytska et al., 2018). Forward trajectories were simulated for 72 h (3 days) at 12:00 UTC starting time, using the normal type of trajectories and GFS meteorological data with a 0.25-degree resolution. In the base settings, the user selects (up to three) starting heights from up to three source locations at the initial time (Draxler et al., 2022). The starting time of 12:00 UTC was chosen to stay close to a sampling of the TROPOMI data. S5P observes the territory of Ukraine in the period from 9:00 UTC to 11:00 UTC dependent on swath width position and orbit.

The model trajectory analysis was combined with the analysis of near-surface weather charts from the German Weather Service (https://www.wetter3.de/archiv_dwd_en.html) to assess the impact of the weather on the processes of transport and dispersion of air pollutants in the atmosphere. In addition, daily data from 24 February to 06 May 2022 for the wind speed and direction from the ECMWF ERA5 reanalysis data were used to provide insight into whether the events with high $NO_2$ tropospheric VCD are emitted by local sources or result from the transport of air masses by the wind. Furthermore, the temperature data from ERA5 for the period of 2019–2022 was also analyzed to observe differences in the characteristics of the temperature regimes during the investigated periods described in Section 2.2.

## 3. Results and discussion

### 3.1. Analysis of $NO_2$ variability over Ukraine in 2019–2022

Fig. 1 shows $NO_2$ tropospheric VCD over Ukraine for the four periods defined in Section 2.2: (a) pre-COVID-19, (b) COVID-19 lockdown, (c) adaptive lockdown, and (d) hostilities. Red contours indicate territories captured by Russian forces as of 31 March 2022, after which a successful counteroffensive began (source: https://liveuamap.com/) and white labels identify administrative centers. The analysis of all pre-hostilities (panels a-c) periods, which represent the specific effects of the COVID-19 lockdown (panels b and c), showed that the most polluted areas in Ukraine are associated with five large industrial zones located close to mines or cities, which have working industries. The largest of them is Donbas, which is located in the east of Ukraine and includes the Donetsk and Luhansk administrative regions. The identification by using $NO_2$ tropospheric VCD is in agreement with the assessment of the National Inventory Report (Lyashenko et al., 2022) and the regional study of the state of air pollution in the period 2018–2020 over Ukraine including remote regions and uncontrolled Ukrainian territories performed by Savenets (2021). Clear maxima of $NO_2$ tropospheric VCD are also linked with the other four industrial zones, namely the Kyiv metropolitan area, industrial cities of Central (Dnipro, Zaporizhzhia) and Western Ukraine (Lviv, Ivano-Frankivsk), and Kharkiv metropolitan area (panels a-c). Although the spatial distribution is similar for all the pre-hostilities periods, the maximum concentration varies as a result of the variability of $NO_x$ emissions to human activities and the large impact of COVID-19 restrictions, which reducing these activities, in particular, $NO_x$ from fossil fuel burning by traffic. The maximum values of $NO_2$ tropospheric VCD amount in the most polluted industrial zone of Donbas were about 6–10 $\times$ $10^{15}$ molec $cm^{-2}$ before COVID-19 (panel a), this reduced to 4–6 $\times$ $10^{15}$ molec $cm^{-2}$ during COVID-19 lockdown (panel b). With the restoration of the transport system during adaptive lockdown (panel c), maximum values of $NO_2$ VCD increased to 6–8 $\times$ $10^{15}$ molec $cm^{-2}$ in Donbas. Our estimates of the changes in $NO_2$ during the COVID-19 lockdown compared to the pre-COVID period (panels a-b) are similar to the differences (−6.0 % ± 1.2%) in the mean TROPOMI $NO_2$ VCDs values estimated by Fioletov et al. (2022). The authors used the method of isolation of three components, namely background $NO_2$, $NO_2$ from urban sources, and $NO_2$ from industrial point sources to estimate the impact of the COVID-19 lockdown on each of these components. The analysis of the hostilities period (panel d) also showed local maxima (3–4 $\times$ $10^{15}$ molec $cm^{-2}$) in the above-mentioned industrial zones and urban agglomerations, but not as intense as in the pre-hostilities period (panels a–c).

To estimate the $NO_2$ VCD changes, which we attribute to the hostilities, Fig. 2 shows the absolute differences between $NO_2$ VCD during hostilities and each of the pre-hostilities period (defined in Section 2.2 and also discussed in Fig. 1a–c). According to Fig. 2, during hostilities satellite measurements of tropospheric $NO_2$ VCD over the industrial zone of Donbas, Kyiv and Kharkiv metropolitan area, and big cities of Dnipro, Zaporizhzhia, Lviv, and Ivano-Frankivsk reveal a temporal decline in $NO_2$ (2–4 $\times$ $10^{15}$ molec $cm^{-2}$) relative to that in all pre-hostilities periods (panels a-c). This result is in good agreement with the study of Zhang et al. (2023), which reported significant $NO_2$ reductions of 10.7–27.3% from 24 February to 7 April 2022, in Ukrainian cities (e.g., Dnipro, Nikopol, Kryvyi Rih), which are on or close to the front line of the confrontation, and also can be observed near red contours in Fig. 2 all panels. At the same time, we also indicated local increases in $NO_2$ tropospheric VCDs values in the northern (Kyiv and Zhytomyr regions), southern (Odesa, Kherson regions), and eastern (Donetsk region) parts of Ukraine ranging from 1 to 4 $\times$ $10^{15}$ molec.$cm^{-2}$ (panels a-c), in contrast to earlier studies, which did not show such an effect. The estimated difference (1–4 $\times$ $10^{15}$ molec.$cm^{-2}$) exceeds the uncertainty associated with the $NO_2$ retrieval process (0.56 ± 0.04 $\times$ $10^{15}$ molec.$cm^{-2}$). We hypothesize that the elevated levels of $NO_2$ could be a consequence of burning activities linked to ongoing hostilities. The increase is not as intensive, because the results in the case of emission from non-stationary sources, like fires, are sensitive to periods of averaging: the larger the averaging period, the more smeared the trace. By averaging the satellite measurements, a track of $NO_2$ near stationary sources like urban areas or industrial units is more stable than a track of fires, which is highly variable in space and time. Even for the events of big fires, the $NO_2$ response might not necessarily be detected given its short tropospheric lifetime, namely within 2–8 h depending on latitude and season (e.g. Fig. 6 in Lange et al., 2022a). Therefore, even a local temporal increase in $NO_2$ VCD suggests that fires were intense for a long time to produce a $NO_2$ VCD increase visible on a 72-day average period.

The variations in $NO_x$ emissions, its transport and transformation can be also attributed to other factors such as seasonality, differences in

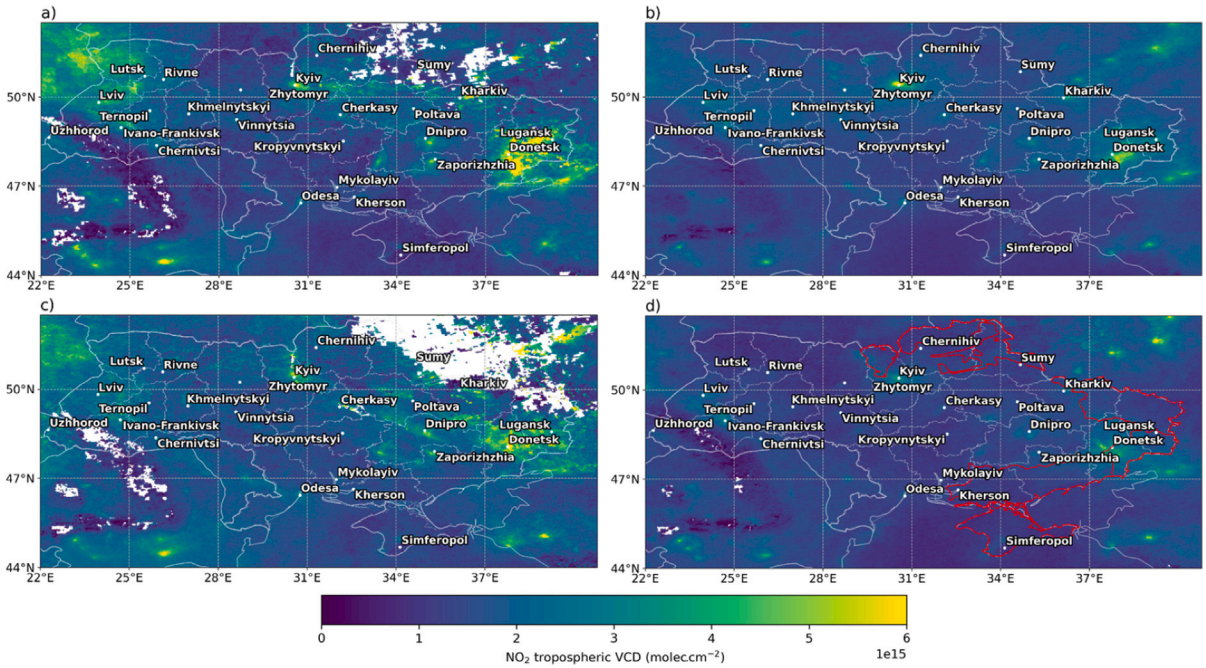


**Fig. 1.** $NO_2$ tropospheric VCD (molec.cm$^{-2}$) distribution during different periods over Ukraine: (a) pre-COVID-19 (31.12.2019–11.03.2020), (b) COVID-19 lockdown (12.03.2020–22.05.2020), (c) adaptive-lockdown (14.12.2021–23.02.2022), (d) hostilities (24.02.2022–06.05.2022) also defined in Section 2.2. Red contours indicate territories captured by Russian forces as of 31 March 2022 (source: https://liveuamap.com/). White labels identify the administrative centers.

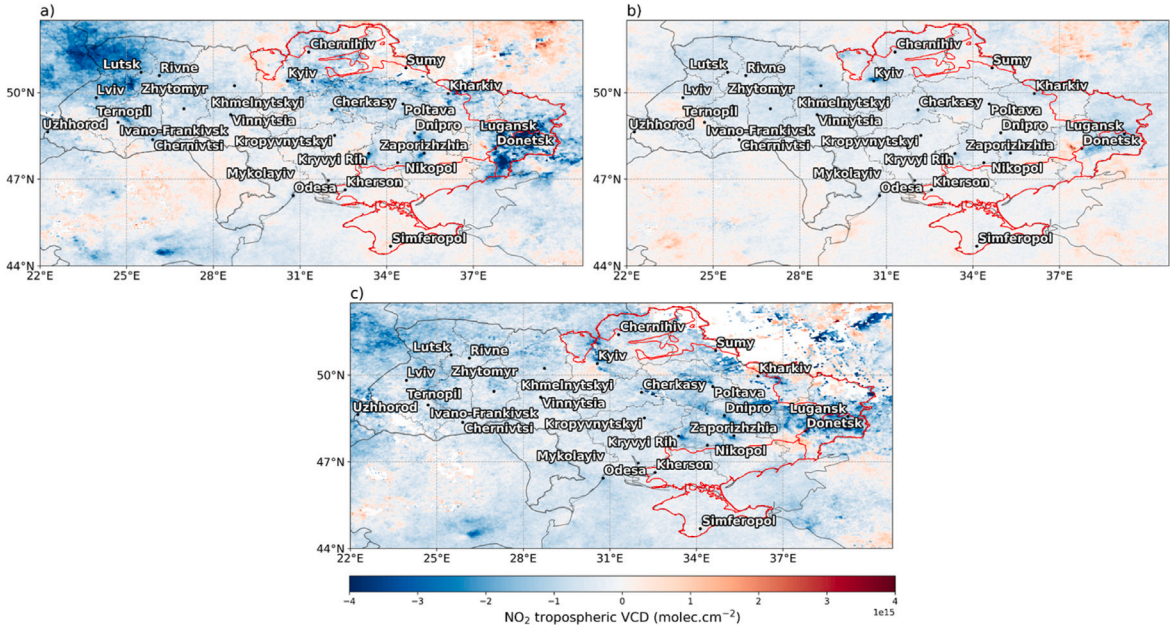


**Fig. 2.** Difference between $NO_2$ VCD (molec.cm$^{-2}$) during the hostilities (24.02.2022–06.05.2022) and (a) pre-COVID-19 period (31.12.2019–11.03.2020), (b) COVID-19 lockdown (12.03.2020–22.05.2020), (c) adaptive lockdown (14.12.2021–23.02.2022). Red lines identify the territories captured by Russian forces as of 31 March 2022.
*Source:* https://liveuamap.com/.

meteorological conditions and fluctuations in temperatures. $NO_2$ intra-annual variations over clean remote regions and industrial zones of Ukraine, based on S5P satellite data for the period of November 2018–January 2020 are presented by Savenets (2021). The authors reported that industrial regions and large cities do not exhibit clear seasonality, however, frequent pollution events and spikes from December to February disrupt the distribution and lead to higher average values in winter. During the seasonal maxima from December to February, the column number density of $NO_2$ reaches 3–5 $\times$ $10^{-4}$ mol m$^{-2}$, while the most stable conditions are observed from June to August and vary somewhat within the range 0.9–1.1 $\times$ $10^{-4}$ mol m$^{-2}$ (e.g. Fig. 3 in Savenets, 2021). For remote clean territories such as the Polissia in the northern part of Ukraine and the Carpathians Mountains, $NO_2$ exhibits seasonal peaks from late May to June, with column number density reaching 0.7–0.8 $\times$ $10^{-4}$ mol m$^{-2}$. Between March and November, $NO_2$ values show low variability, and concentrations typically form under local conditions being minimally influenced by nearby cities or polluted areas. During winter, the $NO_2$ levels drop to around 0.4–0.6 $\times$ $10^{-4}$ mol m$^{-2}$.

Furthermore, as we are comparing averages for specific periods of the year (as mentioned in Section 2.2) to observe differences in

**Table 1**
Mean values of climatic parameters for Ukraine (within 44–52.35°N, 22–40.15°E) averaged for each investigated period according to ERA5 data.

| Parameter | Pre-COVID-19 | COVID-19 | Adaptive lockdown | Hostilities |
|---|---|---|---|---|
| Mean temperature (°C) | 2.6 | 9.4 | −0.1 | 5.8 |
| Min temperature (°C) | −20.0 | −8.8 | −20.7 | −13.7 |
| Max temperature (°C) | 16.6 | 24.9 | 14.8 | 21.1 |
| Mean HDD (°C) | 1111 | 622 | 1300 | 877 |
| Amount of days below 8 °C (days) | 17 | 3 | 33 | 12 |

characteristics of the thermal regime in Table 1 we present the climatic parameters, such as mean, minimum and maximum values of temperature, mean heating degree days (HDD), and the number of days having temperatures below 8 °C, for all investigated periods averaged for Ukraine (44–52.35°N, 22–40.15°E). The latter parameter is used in Ukraine as an indicator of the duration of the heating season, as this temperature threshold (8 °C) generally represents the point at which buildings require heating. HDD is defined as the number of degrees Celsius a given day's mean temperature is below 18 °C. The resulting daily HDD values are summarized for the period and averaged by area. The higher HDD values imply that more heating is required to maintain a comfortable indoor temperature, which in turn implies higher energy consumption and more air pollutant, emitted from combustion processes, including $NO_x$ and $NO_2$. Table 1 shows that the adaptive lockdown period was the coldest among all investigated periods during which the mean temperature in Ukraine was −0.1 °C. The minimum temperature during the adaptive lockdown was −20.7 °C, indicating that this period was characterized by extreme cold events. The number of days with temperatures below 8 °C during the adaptive lockdown period was 33, which is the highest among all investigated periods, indicating the longest heating season. The mean HDD was 1300 °C, which also indicates a higher demand for heating compared to other investigated periods.

The climatic parameters during the adaptive lockdown period were most similar to those during the pre-COVID-19 period. As shown in Table 1, the mean temperature during the pre-COVID-19 was 2.6 °C, which is higher, but still the closest to the mean temperature during the adaptive lockdown period (−0.1 °C). Moreover, the mean HDD value was 1111 °C, which is also comparable to the mean HDD during the adaptive lockdown period (1300 °C). Despite this, the highest $NO_2$ VCDs were observed during pre-COVID-19 period (6–10 × $10^{15}$ molec $cm^{-2}$, as shown in Fig. 1 panels a-d) that suggest other factors, beyond climatic parameters and heating demands, may have played a role in the observed differences in $NO_2$ VCD between these periods. During hostilities, the thermal regime in Ukraine was relatively mild, with a mean temperature of 5.8 °C and a minimum temperature of −13.7 °C, which is less extreme than during the pre-COVID-19 and adaptive lockdown periods. Moreover, the mean HDD was 877 °C, which is also comparable to the COVID-19 period, but lower than during other periods, suggesting a relatively lower demand for heating.

Thus, the local increases in $NO_2$ tropospheric VCDs values during hostilities in the northern (Kyiv and Zhytomyr regions), southern (Odesa, Kherson regions), and eastern (Donetsk region) parts of Ukraine shown in Fig. 2 are primarily related to non-industrial regions, and they cannot be attributed to seasonality or to the combustion of fossil fuels used for heating. We suggest this elevated $NO_2$ may be a product of burning caused by active fights. It should be noted that since 2014 Donbas, the most polluted territory of Ukraine, has temporarily remained out of the control of the Government of Ukraine.

### 3.2. Assessment of fire's influence on $NO_2$ emission in 2022 over Ukraine

A notable number of fires of both natural and human-made origin have been recorded since hostilities started, causing air pollution. The time series of the total number of fire pixels per month averaged for Ukraine are shown in Fig. 3 (panel a). It considers both daytime and nighttime measurements, with a confidence value above 80% (see Section 2.3). A comparison of the number of fires in 2022 (orange) within the same periods of the previous year 2021 (blue) shows that during almost all analyzed months of 2022, there was a higher number of fires in comparison with 2021, except April, August, and September. The decrease in the number of fires in these months may be related both to a decrease in the intensity of hostilities and to the tradition of burning vegetation in the fields before sowing (April) or after harvesting (August–September). According to Fig. 3a, in general, for Ukraine, the highest ratio (11.1) of the frequency of fires in 2022 compared to 2021 was recorded in March, when the full-scale hostilities started. The total amount of fire pixels registered by satellite in March 2022 is 11.1 times more than likewise numbers for 2021 (613 and 55 cases of fire pixels, respectively).

The daily variations in the number of fire pixels, as well as its daily average and maximum values of FRP in Ukraine for the hostilities period, are shown in Fig. 3b for the first 72 days of hostilities. With blue vertical bars, we show three periods of bursts in a number of fires, spatially and temporally related to hostilities (supported by data from https://liveuamap.com/): 19–30 March, 24–28 April, and 3–6 May. The largest number of fires and the highest FPR values were observed during 19–30 March. During this period we found three separate localized clusters of fires associated with episodes of high pollution levels. We indicate bursts of fires on the north border of the Kyiv and Zhytomyr regions, including part of the Chornobyl Exclusion Zone on 19–23 March, on the front-line Pisky–Maryinka–Starognativka (Donetsk region) on 21–26 March, and on the Danube biosphere reserve, on 28–30 March, as shown in Fig. S1a in the supplement. During 24–28 April, the fires were located near the towns of Rubizhne, Kreminna, and Severodonetsk in the Lugansk region (Fig. S1b in the supplement). During 3–6 May the fires were detected at Kinburn spit regional landscape park in the Mykolaiv region and near the towns of Lyman and Yaremivka, which are situated on the border of the Kharkiv and Lugansk regions (Fig. S1c in the supplement).

Table 2 presents the monthly amount of fire pixels for the first nine months of 2022, which coincides with the time of ongoing hostilities for each region of Ukraine. Administrative regions in which hostilities were conducted in March 2022, based on data from https://liveuamap.com/, are highlighted in bold. Table 2 demonstrates that during January–September 2022 the highest total number of fires is detected mostly over the east (Donetsk region) and south Ukraine (Kherson, Mykolaiv, and Zaporizhzhia regions). In particular, the highest number of fire pixels in Ukraine was detected in the Kherson and Mykolaiv regions in July (186 and 160 fire pixels correspondingly) and in the Donetsk region in July (119) and August (144). Such a high number of fire pixels is outstanding compared to other analyzed months and other regions of Ukraine. The lowest number of fire pixels is detected mostly over the western (Volyn, Rivne, Ternopil regions), central (Vinnytsia, Zhytomyr, Cherkasy, Poltava regions), northern (Sumy region) parts of Ukraine and Crimea. In March 2022, despite the presence of hostilities in the Sumy region, the number of fires in the region was relatively low. According to data from "Liveuamap" (also described in Section 2.2), this could be attributed to a lower incidence of heavy shelling compared to other areas. Below we focus on the fire events, associated with the active hostilities in Ukraine supported by data from https://liveuamap.com/. In March, as a direct consequence of active hostilities the highest number of fire pixels was detected in the Donetsk (99), Kyiv (59), and Lugansk regions (42). The study of the localization of fire's pixels

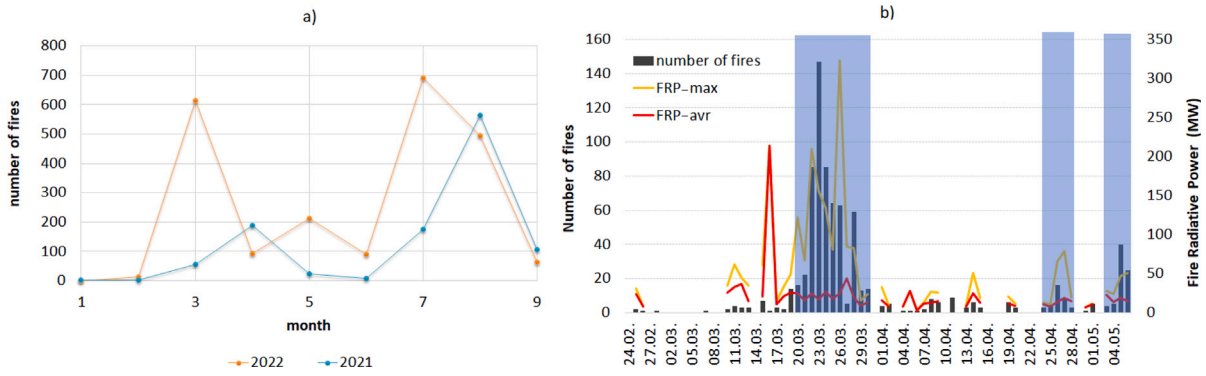


**Fig. 3.** (a) Temporal distribution of the number of fire pixels in Ukraine in 2021–2022 and (b) daily variations in the number of fire pixels and the daily average (FRP-avr) and maximum (FRP-max) FRP values in Ukraine for the hostilities period. The blue vertical bars indicate the periods of the increased number of fires.

**Table 2**
Total amount of fire pixels over Ukraine during January–September 2022 according to VIIRS data. Bold stands for the administrative regions where hostilities were conducted in March 2022.

| Region | JAN | FEB | MAR | APR | MAY | JUN | JUL | AUG | SEP | Total |
|---|---|---|---|---|---|---|---|---|---|---|
| Vinnytsia | 0 | 0 | 23 | 8 | 0 | 0 | 1 | 1 | 0 | 33 |
| Volyn | 0 | 0 | 11 | 1 | 2 | 0 | 0 | 0 | 0 | 14 |
| Dnipro | 0 | 1 | 31 | 1 | 2 | 6 | 14 | 14 | 1 | 70 |
| **Donetsk** | 0 | 2 | 99 | 13 | 24 | 7 | 119 | 144 | 10 | 418 |
| Zhytomyr | 0 | 0 | 36 | 1 | 7 | 0 | 0 | 2 | 3 | 49 |
| Zakarpattia | 0 | 0 | 26 | 0 | 0 | 0 | 2 | 2 | 0 | 30 |
| **Zaporizhzhia** | 0 | 3 | 11 | 3 | 4 | 1 | 91 | 89 | 16 | 218 |
| Ivano-Frankivsk | 0 | 0 | 25 | 4 | 0 | 0 | 0 | 0 | 0 | 29 |
| **Kyiv** | 0 | 0 | 59 | 3 | 29 | 1 | 0 | 20 | 4 | 116 |
| Kirovohrad | 0 | 0 | 28 | 3 | 5 | 0 | 4 | 4 | 0 | 44 |
| **Lugansk** | 0 | 1 | 42 | 16 | 20 | 15 | 40 | 28 | 10 | 172 |
| Lviv | 0 | 0 | 36 | 1 | 0 | 0 | 1 | 1 | 0 | 39 |
| **Mykolaiv** | 0 | 0 | 14 | 0 | 0 | 15 | 160 | 40 | 1 | 230 |
| Odesa | 1 | 3 | 61 | 13 | 3 | 1 | 42 | 16 | 12 | 152 |
| Poltava | 0 | 0 | 9 | 0 | 3 | 2 | 0 | 1 | 0 | 15 |
| Rivne | 0 | 0 | 6 | 0 | 7 | 0 | 0 | 1 | 0 | 14 |
| **Sumy** | 0 | 0 | 1 | 0 | 1 | 1 | 0 | 2 | 0 | 5 |
| Ternopil | 0 | 0 | 10 | 0 | 0 | 1 | 0 | 0 | 0 | 11 |
| **Kharkiv** | 0 | 0 | 25 | 11 | 16 | 28 | 29 | 28 | 0 | 137 |
| **Kherson** | 0 | 2 | 6 | 7 | 51 | 10 | 186 | 91 | 6 | 359 |
| Khmelnytskyi | 0 | 0 | 8 | 1 | 4 | 0 | 1 | 2 | 0 | 16 |
| Cherkasy | 0 | 0 | 7 | 0 | 8 | 0 | 0 | 0 | 0 | 15 |
| Chernivtsi | 0 | 0 | 14 | 2 | 3 | 0 | 0 | 0 | 0 | 19 |
| **Chernihiv** | 0 | 1 | 24 | 0 | 23 | 2 | 0 | 3 | 0 | 53 |
| Crimea | 0 | 0 | 1 | 3 | 0 | 0 | 1 | 2 | 1 | 8 |
| Ukraine (total) | 1 | 13 | 613 | 91 | 212 | 90 | 691 | 491 | 64 | 2266 |

shows that fire is three times more frequent phenomenon in hostilities-related areas, compared to neighboring territories (also shown in Fig. S2 panels a-i in the supplement). This is consistent with patterns described for the hostilities in the ATO zone of Ukraine in June–September 2014 (Vasyliuk et al., 2015). In particular, in the Donetsk region, where hostilities are constantly taking place, the number of fires is higher than in the Dnipro region, which borders the Donetsk region in the west, and has the same climate conditions but there is no front line. Consequently, during 2022 fire activities increased significantly in the active hostilities area, especially in the warm period.

To demonstrate that the observed increase in $NO_2$ concentration is indeed linked to fire activities resulting from hostilities, we additionally analyzed the daily averaged flux of $NO_x$ originating from fires and biomass burning, based on GFAS data. Fig. 4 represents the aggregated $NO_x$ emissions over the period of increased fire incidents (19-30.03.2022), previously detailed in Fig. 3b. During this timeframe, numerous fires of varying intensities were recorded in Ukraine and neighboring countries. The majority of recorded fires exhibited total emissions up to $0.5 \times 10^{-9}$ kg m$^{-2}$ s$^{-1}$. However, three distinct fire clusters, attributed to active conflicts, in the Chornobyl Exclusion Zone, along the front-line in Pisky–Maryinka–Starognativka (Donetsk region), and within the Danube biosphere reserve displayed emissions at a significantly higher rate of $2 \times 10^{-9}$ kg m$^{-2}$ s$^{-1}$, as also determined earlier from VIIRS instrument data and illustrated in Fig. S1a in the supplement. The significantly higher emission rates of $NO_x$ in these fire clusters highlight the impact of hostilities on the observed increase in $NO_2$ VCDs. To complement this evaluation, we also calculated daily values of fire flux of $NO_x$ over the Kyiv region, averaged by territory (within 50–52.35°N, 28–31°E). The maximum total emissions of $NO_x$ in the Kyiv region were observed during 19–23 March and reached up to $8.6 \times 10^{-9}$ kg m$^{-2}$ s$^{-1}$. Furthermore, we verified the plume's top height above the surface within Ukraine. Fires associated with isolated incidents, such as one-off strikes (see Frederick et al., 2022) or burning vegetation in fields, exhibited plume top heights around 1000–1500 m. However, fires driven by heavy shelling or active fights reached up to 2000 m and higher, with the maximum recorded height being 3700 m near Maryinka city in the Donetsk region as shown in Fig. S3 in the supplement.

To investigate whether increased fire activities contribute to pollution at both local and regional levels, we provide a case-study of a fire episode of 19–23 March 2022 in the Kyiv region, as mentioned in Section 2.3, using HYSPLIT simulation.

### *3.3. Case-study on a fire distribution and $NO_2$ VCDs on 19–23 March 2022 in the Kyiv region*

During 19–23 March 2022 the main emission of $NO_2$ VCDs (over $4 \times 10^{15}$ molec cm$^{-2}$) was observed in the north of the Kyiv region, mainly from two centers. One of them was located at the Chornobyl Exclusion Zone (51.21°N, 29.30°E) and bordered in the northwest by the Zhytomyr region, the other one was located near Bucha (50.54°N, 30.28°E) to the southeast of Irpin and Hostomel cities. The location of both centers is shown in Fig. S4 in the supplement. VIIRS satellite instrument detected about 26 fire locations around the Chornobyl Exclusion Zone and 13 fire spots around Bucha (see Fig. S4 panels a-e in the supplement) during 19–23 March 2022. Fig. 5 represents the time series of $NO_2$ VCD over the Chornobyl Exclusion Zone and Bucha during the period of hostilities. The teal vertical bars indicate the periods with the increased number of fires, which agrees with Fig. 3b. Fig. 5 shows significant temporal dynamics of $NO_2$ VCD with pronounced peaks during 19–20 March at the Chornobyl Exclusion Zone (panel a) and on 23rd March near Bucha (panel b). In the Chornobyl Exclusion Zone, $NO_2$ VCD was higher than near Bucha city because the number of fires over this area was twice higher (26 fire pixels) than over Bucha (13 fire pixels). If the daily $NO_2$ tropospheric VCDs in the Chornobyl Exclusion Zone increased from 2.5 to $8.7 \times 10^{15}$ molec cm$^{-2}$ with the start of fires, reaching a maximum of $17.5 \times 10^{15}$ molec cm$^{-2}$ on 20 March 2022 (panel a), in Bucha the increase of $NO_2$ was a factor of two smaller, and daily values did not exceed $7 \times 10^{15}$ molec

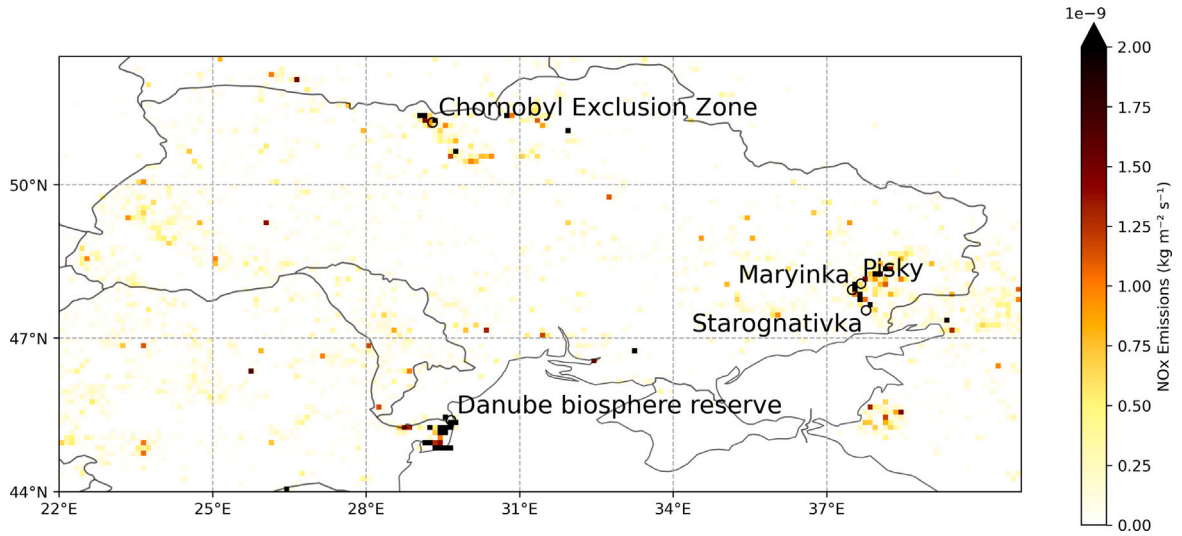


**Fig. 4.** Spatial distribution of the total $NO_x$ emissions from fires and biomass burning averaged over the period of heightened fire activities (19-30.03.2022), as derived from GFAS data.

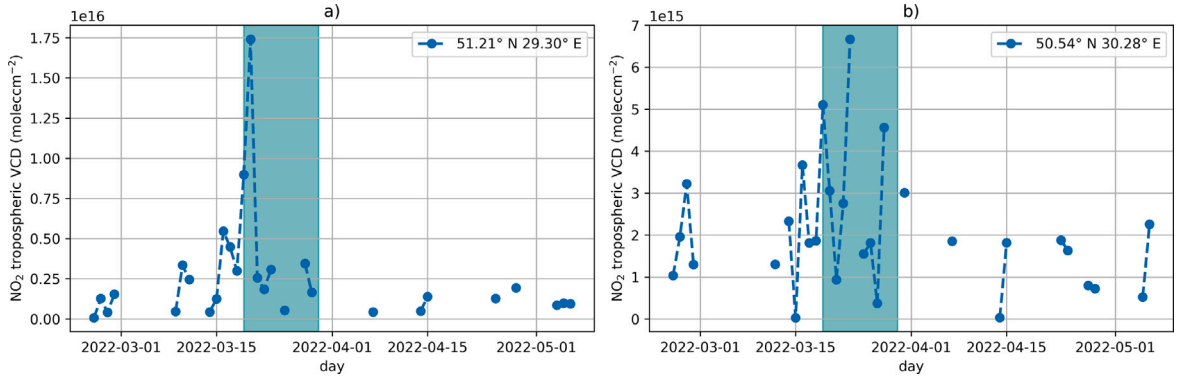


**Fig. 5.** Daily $NO_2$ VCD over two centers of fire in the Kyiv region during hostilities period (24.02.-06.05.2022): (a) Chornobyl Exclusion Zone - 51.21°N 29.30°E, (b) near Bucha city - 50.54°N 30.28°E. The teal vertical bars represent the period of the increased number of fires (19-30.03.2022), which agrees with Fig. 3b.

$cm^{-2}$ (panel b). Nevertheless, the abundance of $NO_2$ at both centers is comparable to the most polluted Ukrainian industrial cities during the pre-COVID-19 period (shown in Fig. 1a). Fig. 6 illustrates the distribution of $NO_2$ tropospheric VCD, fires location and FRP, wind speed, and wind direction over Ukraine on 20 March 2022, a day when daily $NO_2$ concentrations reached their maximum in the Chornobyl Exclusion Zone. As it is particularly evident from Fig. 6, the $NO_2$ plumes, traced by the TROPOMI satellite instrument, are local (around 50 km footprint). This is in good agreement with a study of Savenets et al. (2020), which investigated the influence of wildfires that occurred in the northern part of Ukraine during April 2020, on changes of CO, $NO_2$ and the aerosol index. The authors reported that at a distance of 50 km from the fires, the content of CO in the atmosphere decreased by 2–3 times, and $NO_2$ by 10 times. Most affected areas were within 50 km of active fires, depending on the wind speed and direction. Abnormally dry weather conditions also contributed to the occurrence and spread of fires in March 2022. Based on the monthly weather reports of the Ukrainian Hydrometeorological Center, March 2022 was drier than the average (44 mm,1981–2010) for the whole country. Ukraine as a whole had 21%–79% of average rainfall, and in some areas of the northwest fell only 2%–20% of the monthly norm. Meanwhile, above-average precipitation (1–1.5 norm) occurred only in the north of the Lugansk region. An analysis of weather charts from the German Weather Service (see Fig. S5 panels a-l in the supplement) showed that on 20–23 March (panels b-e), weather without precipitation was determined by the crests of a high anticyclone over the Baltic Sea, which moved in a southeast direction. Stable weather conditions, corresponding to anticyclonic circulation, caused the accumulation of $NO_2$ VCD up to $17.5 \times 10^{15}$ molec $cm^{-2}$ from fires over the Kyiv region. However, from 23 to 24 March, the weather conditions changed. On 24–28 March (panels f-j), cyclone and atmospheric fronts from the northwest resulted in rain and windy weather in the northern half of the country. This change likely caused a decrease in fire activities and a wet deposition of pollutants, lowering $NO_2$ content to $2–3.5 \times 10^{15}$ molec $cm^{-2}$ in the atmosphere above Ukraine. Thus, the analysis of weather charts, combined with TROPOMI and VIIRS satellite data, indicates that high air pollution levels on 19–23 March 2022 were caused by local air pollution sources, namely fires, and not by short- and long-distance transport of air masses. In our analysis below, we focus on the transboundary and regional transport of pollutants from the fires at the Chornobyl exclusion zone and near Bucha city, using the HYSPLIT model version 5.2 (see Section 2.5). We calculated HYSPLIT version 5.2 forward trajectories for 72 h for the dates of maximum $NO_2$ VDC for each center from Fig. 5. Each subsequent point in Fig. 7 shows the position of the air mass six hours after fixing the previous position.

According to the forward trajectories simulation of the HYSPLIT model, on 20 March, combustion products with a starting altitude of 530 m, were transported outside of the Chornobyl Exclusion Zone to other regions of Ukraine in the southwest direction within the first 12 h, and through Romania, Serbia, Kosovo, and Albania towards Mediterranean sea afterwards (Fig. 7a, red). Air movements at starting altitudes of 1.5 km and 3 km corresponded to anticyclonic circulation,

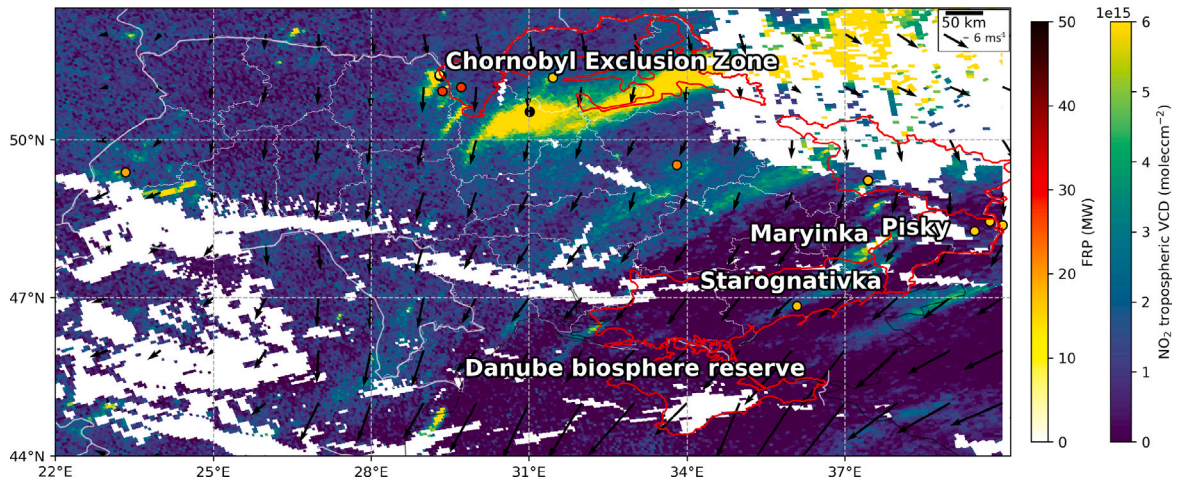


**Fig. 6.** Spatial $NO_2$ VCDs and fire distribution over Ukraine on 20 March 2022. Circles identify the fire locations, black arrows indicate wind speed and direction. Labels stand for the locations near clusters of fires indicated during 19–30 March 2022 also shown in Fig. S1 panels a-c in the supplement.

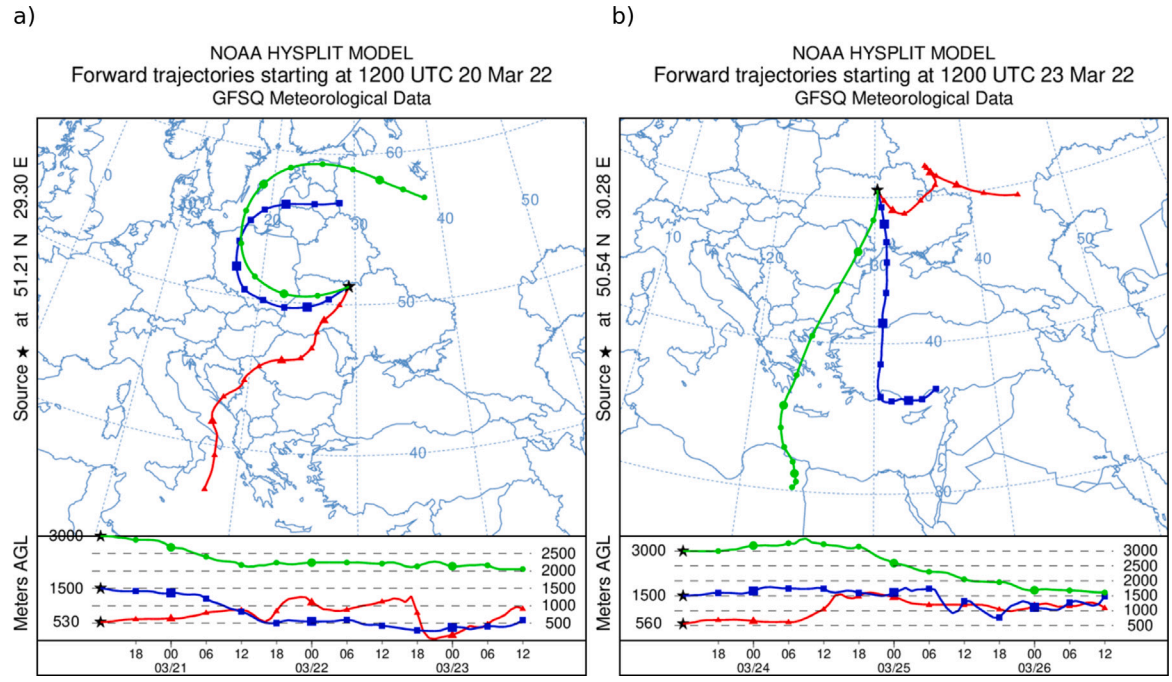


**Fig. 7.** Forward trajectories of air masses, based on HYSPLIT model version 5.2, from the centers of fire (a) Chornobyl Exclusion Zone - 51.21°N 29.30°E, (b) near Bucha city - 50.54°N 30.28°E for the dates of maximum concentration $NO_2$ shown in Fig. 4.

which is seen in Fig. 7 (panel a, blue and green correspondingly) as clockwise-shaped curves. It revealed that at the height of 1.5–3 km, a smoke-particle-included air mass with increased $NO_2$ ($17.5 \times 10^{15}$ molec $cm^{-2}$, as shown in Fig. 5b), from the fire center at the Chornobyl Exclusion Zone was extended to Poland and countries of the Baltic region. At 2 km height, the air mass reached the Russian Federation in 72 h.

Forward trajectories near Bucha, where the maximum $NO_2$ VCD was observed on 23 March, are shown in Fig. 7b. The trajectories indicate that with the starting altitude of 560 m in the lower troposphere within the first 12 h, the northwest wind spread the $NO_2$-rich air to Kyiv and Cherkasy regions and then returned to the northeast towards the Russian Federation. Smoke related to the fires near Bucha city on 23 March was observed at a distance of about 200 km downwind of the fire, covering the area of Kyiv city. At 1.5 km altitude, air mass with increased $NO_2$ content was transported towards the Black Sea and the Republic of Turkey, but at the 3 km layer of the troposphere, the air parcels were transported to Moldova, Romania, Bulgaria, and Greece.

The next step was to examine whether there was indeed confirmed increased air pollution in the areas expected to be affected according to forward trajectories simulation (Fig. 7) by analyzing the variation in $NO_2$ VCDs between the day of the fire outbreak and the subsequent day. Fig. 8 visually presents these variations, depicting the $NO_2$ VCD differences on both March 20 and 21, 2022 (panel a), and March 23 and 24, 2022 (panel b). Additionally, the figure incorporates the trajectories predicted by the HYSPLIT model version 5.2, originating from the fire centers, as also shown in Fig. 7. The red-marked circle corresponds to the location of the air mass after 24 h following the starting time (12:00 UTC on 20 March 2022, panel a, and 12:00 UTC on 23 March 2022 panel b) at 1.5 km altitude. Fig. 8 unveiled a visible difference in $NO_2$ VCD levels, indicating an increase to around 0.5–1.0 $\times 10^{15}$ molecules $cm^{-2}$ in Poland following the fire event at the Chornobyl Exclusion Zone at 1.5 km altitude. This result is consistent

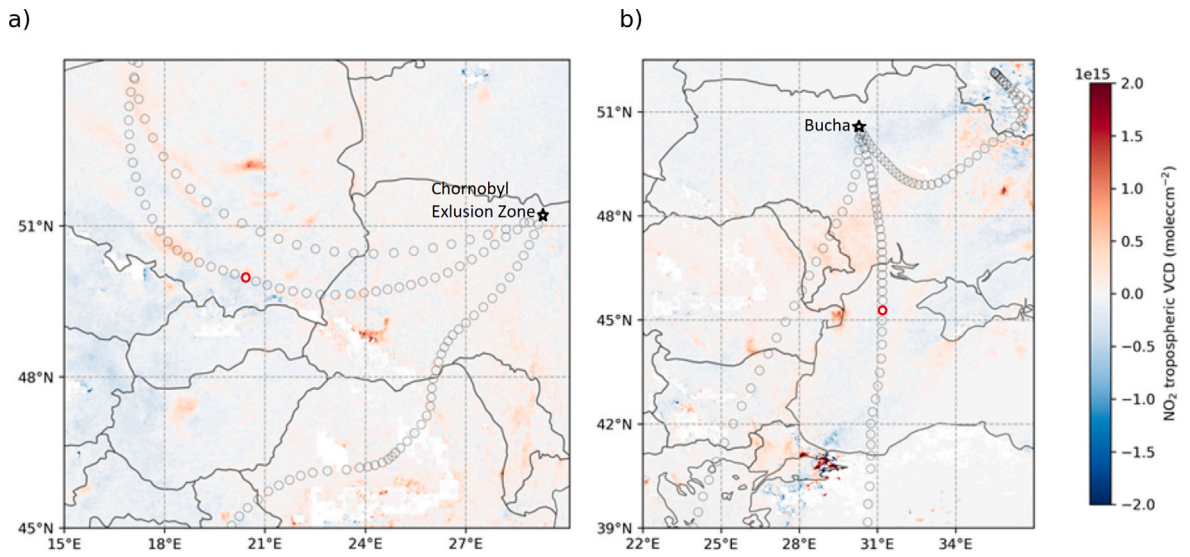


**Fig. 8.** Difference of $NO_2$ VCDs on (a) 20 and 21 March 2022 and (b) 23 and 24 March 2022. Gray circles indicate the position of air mass every hour after starting time (12:00 UTC on 20 March 2022 for panel a, and 12:00 UTC on 23 March 2022 for panel b). The red-marked circles indicate the location of the air mass after 24 h following the starting time at 1.5 km altitude.

with the findings presented by Wieczorek (2023), which identified an increased $NO_2$ (+0.67 ± 0.47 μmol/m$^2$) in Poland due to the ongoing military operations in Ukraine. However, in the case of fires near Bucha (shown in Fig. 8 panel b), where the release in $NO_2$ was half as large as comparable with Chornobyl Exclusion Zone, no observed increase in $NO_2$ over the Black Sea was evident.

## 4. Conclusions

In this study, we investigate the extent to which the hostilities resulting from the invasion of Ukraine by Russia affect air quality in Ukraine, by studying its effect on the abundance, dynamics, and spatiotemporal distribution of the $NO_2$ tropospheric VCD, retrieved from the TROPOMI instrument for the period 24 February–6 May 2022. In addition, the analysis was also made for periods in 2019, 2020, and 2021 to analyze the $NO_2$ tropospheric VCD variability before the hostilities and to differentiate the effects of COVID-19 restrictions and the hostilities on $NO_2$ emissions over Ukraine. In addition to available studies on the spatial and temporal responses of $NO_2$ to the Russia–Ukraine armed conflict in 2022 over Ukraine, Poland, and Russia (Zhang et al., 2023; Wieczorek, 2023), we study fire distribution and its intensity, both confirm their influence on the tropospheric $NO_2$ level and explore the impact of the hostilities on fire frequency over Ukraine. Furthermore, we analyzed the $NO_x$ emission and injection altitude of fires using the GFAS wildfire emission inventory to validate the impact of hostilities on atmospheric pollution processes, resulting from the increased frequency and intensity of fires in conflict zones. To confirm that the fires under investigation were indeed caused by hostilities, we additionally analyzed data from livemap.ua. Finally, we analyzed the transborder and regional air mass transport from the origin of the fires using the HYSPLIT model version 5.2, supplemented with an analysis of near-surface weather charts, which has not been done before.

Our comparison of $NO_2$ VCD values before and during hostilities showed that hostilities resulted in an unprecedented reduction in economic activity, comparable to the COVID-19 pandemic lockdown, and correspondingly, temporarily reduced $NO_2$ emission over the industrial zone of Donbas, Kyiv and Kharkiv metropolitan area, and large cities or urban agglomerations of Dnipro, Zaporizhzhia, Lviv, and Ivano-Frankivsk on 2–4 × $10^{15}$ molec cm$^{-2}$ relative to the analyzed pre-hostilities periods. While for the majority of Ukraine, we show that the $NO_2$ amount declined due to hostilities, we also detect local increases in $NO_2$ tropospheric VCD values in the northern (Kyiv and Zhytomyr regions), southern (Odesa, Kherson regions), and eastern (Donetsk region) regions of Ukraine ranging from 1 to 4 × $10^{15}$ molec cm$^{-2}$. We attribute these increases of $NO_2$ with fire events, associated with the active hostilities in Ukraine supported by data from https://liveuamap.com/.

The spatial distribution of fire detected by the VIIRS instrument during Januaries–Septembers 2021–2022 revealed that there was a higher number of fires in 2022 in comparison to 2021 except for April, August and September. In particular, the hostilities significantly increased the number of fires in the eastern, central, and southern parts of Ukraine. The total amount of fire pixels registered by satellite in March 2022, when the full-scale hostilities started in Ukraine, was 11.1 times more than that for 2021, which amounted to 613 and 55 cases of fire, respectively. The highest number of fire pixels (i.e. 691 fire pixels) in Ukraine was detected in July, particularly in the Kherson, Mykolaiv, and Donetsk regions (186, 160, and 119 fire pixels correspondingly). The number of fires increased not only due to hostilities but also due to the beginning of the fire season and rising temperatures. With the recent increase in fires, the threat to air quality is also increasing. We indicated and discussed three periods of bursts in the number of fires, spatially and temporally related to hostilities: i.e. 19–30 March, 24–28 April, and 3–6 May 2022. The analysis of the daily averaged flux of $NO_x$ originating from fires and biomass burning, based on GFAS data, showed that fire clusters in conflict zones had four times higher $NO_x$ emission rates (i.e. 2 × $10^{-9}$ kg m$^{-2}$ s$^{-1}$) compared to fires located far from the front line or resulting from isolated strikes. The plume heights of these fires reached up to 2–3 km or the isobaric surface of 850–700 hPa suggesting that the released pollutants have the potential to disperse and be transported over considerable distances in the troposphere.

The case-study of the fire distribution and $NO_2$ VCDs in the Kyiv region during 19–23 March 2022, when the largest number of fires was observed, clearly demonstrates that as a direct consequence of hostilities, $NO_2$ emissions increased due to the increase in fires. The intensive forest fires over the Chornobyl Exclusion Zone and near Bucha city on 19–23 March 2022 created elevated amounts of $NO_2$ (17.5 × $10^{15}$ molec cm$^{-2}$ and 7 × $10^{15}$ molec cm$^{-2}$), which are comparable to the most polluted Ukrainian industrial cities during the pre-COVID-19 period (shown in Fig. 1a). The analysis of forward HYSPLIT version 5.2 trajectories showed that the air mass with increased $NO_2$ content from the Chornobyl Exclusion Zone was transported to Poland and countries

of the Baltic region at the altitudes of 1.5–3 km. In the lower 530 m layer of the troposphere, a smoke-particle-included air mass was carried outside the Chornobyl Exclusion Zone to other regions of Ukraine in the southwest direction within the first 12 h, and through Romania, Serbia, Kosovo, and Albania and then towards the Mediterranean sea. The most affected territories were within 50 km of active fires (traced $NO_2$ plume is around 50 km footprint), but air quality deterioration was also observed at a distance of about 200 km downwind. A visible trace of $NO_2$, which originated from fires in the Chornobyl Exclusion Zone on March 20, 2022, was observed in Poland the following day.

Further studies are needed to investigate the influence of a significantly increased number of fires on the air quality over eastern and southern parts of Ukraine in July 2022, which also belongs to another natural zone according to Physical Geographical zoning. In our study, we were unable to address this issue due to the release of a new version (V02.04.00) of the TROPOMI Level 2 $NO_2$ data product on 20 July 2022, which introduced significant changes from the version (V02.03.01) used in the current study. Additionally, a comparison with a chemistry-transport model (CTM) can also be made to gain more insights into the transport and transformation of pollutants in the atmosphere and to compare with the results obtained from the satellite observations. Moreover, adding other gases ($SO_2$, CO) and aerosols to the analysis could help identify additional sources and extent of air pollution caused by the hostilities as well as its influence on public health.CALIOP aerosol observations, for instance, could provide valuable insights for the analysis of air pollutants emissions and their transport due to hostilities. Furthermore, the discovery of techniques for extracting $NO_x$ emissions from TROPOMI data, with a specific focus on refineries, could have a crucial impact on similar studies and represent an alternative area for further research. For instance, de Foy and Schauer (2022) application of the flux divergence method and a Gaussian Mixture Model, based on TROPOMI data, to identify peak $NO_x$ emission hotspots over four megacities in South Asia exemplifies the potential of such methodologies.

## CRediT authorship contribution statement

**Liudmyla Malytska:** Formal analysis, Visualization, Writing – original draft, Writing – review & editing, Methodology. **Annette Ladstätter-Weißenmayer:** Methodology, Supervision. **Evgenia Galytska:** Investigation, Methodology, Writing – original draft, Writing – review & editing. **John P. Burrows:** Conceptualization, Writing – review & editing.

## Declaration of competing interest

The authors declare that they have no known competing financial interests or personal relationships that could have appeared to influence the work reported in this paper.

## Code and data availability

The TROPOMI $NO_2$ product is publicly available from Copernicus Data Space Ecosystem and on the S5P-PAL data portal (https://dataspace.copernicus.eu/). The reprocessed (S5P-PAL) and offline (S5P-OFFL) version V02.03.01 data were used in this study. The VIIRS Active Fire and Thermal Anomalies product is available from NASA FIRMS at https://earthdata.nasa.gov/firms. The GFAS data is currently accessible through the Atmosphere Data Store (ADS) as CAMS global biomass burning emissions based on fire radiative power (GFAS) dataset (https://ads.atmosphere.copernicus.eu/cdsapp#!/dataset/cams-global-fire-emissions-gfas) The European Centre for Medium-Range Weather Forecasts (ECMWF) ERA5 reanalysis data are available from https://www.ecmwf.int/en/forecasts/datasets/reanalysis-datasets/era5. The near-surface weather charts are from the German Weather Service https://www.wetter3.de/archiv_dwd_en.html. The HYSPLIT model version 5.2 is available at https://www.ready.noaa.gov/HYSPLIT.php. The HYSPLIT model version 5.2 can be run interactively on the READY website or installed on a PC (Mac, Windows or LINUX operating systems).

## Acknowledgments

The authors gratefully acknowledge the NOAA Air Resources Laboratory (ARL) for the provision of the HYSPLIT transport and dispersion model and/or READY website (https://www.ready.noaa.gov) used in this publication. LM would like to acknowledge the Ukrainian Hydrometeorological Center for providing the monthly weather report and German Weather Service for supplying weather charts. LM would like to express sincere gratitude to the IUP DOAS group for collaboration and valuable discussion of the paper during the seminars. LM is funded by a grant of Volkswagen-Stiftung Funding for Refugee Scholars and Scientists from Ukraine. EG is supported by Central Research Development Fund at the University of Bremen, Funding No: ZF04A/2023/FB1/Galytska Evgenia.

## Appendix A. Supplementary data

Supplementary material related to this article can be found online at https://doi.org/10.1016/j.atmosenv.2023.120281.

## References

Alvarado, L.M.A., Richter, A., Vrekoussis, M., Hilboll, A., Kalisz Hedegaard, A.B., Schneising, O., Burrows, J.P., 2020. Unexpected long-range transport of glyoxal and formaldehyde observed from the Copernicus Sentinel-5 precursor satellite during the 2018 Canadian wildfires. Atmos. Chem. Phys. 20 (4), 2057–2072. http://dx.doi.org/10.5194/acp-20-2057-2020, URL: https://acp.copernicus.org/articles/20/2057/2020/.

Andela, N., Kaiser, J., Heil, A., van Leeuwen, T., van der Werf, G., Wooster, M., Remy, S., Schultz, M., 2013. Assessment of the Global Fire Assimilation System (GFASv1), MACC-II (monitoring atmospheric composition and climate) project. In: Technical Memorandum No. 702. ECMWF.

Barnaba, F., Angelini, F., Curci, G., Gobbi, G.P., 2011. An important fingerprint of wildfires on the European aerosol load. Atmos. Chem. Phys. 11 (20), 10487–10501. http://dx.doi.org/10.5194/acp-11-10487-2011.

Bodhaine, B., Harris, J., Ogren, J., Hofmann, D., 1992. Aerosol optical properties at Mauna Loa Observatory: Long-range transport from Kuwait? Geophys. Res. Lett. 19 (6), 581–584. http://dx.doi.org/10.1029/92GL00524.

Bondur, V., Tsidilina, M., Kladov, V., Gordo, K., 2019. Irregular variability of spatiotemporal distributions of wildfires and emissions of harmful trace gases in Europe based on satellite monitoring data. In: Doklady Earth Sciences, Vol. 485. Springer, pp. 461–464. http://dx.doi.org/10.1134/S1028334X19040202.

Bovchaliuk, A., Milinevsky, G., Danylevsky, V., Goloub, P., Dubovik, O., Holdak, A., Ducos, F., Sosonkin, M., 2013. Variability of aerosol properties over Eastern Europe observed from ground and satellites in the period from 2003 to 2011. Atmos. Chem. Phys. 13 (13), 6587–6602. http://dx.doi.org/10.5194/acp-13-6587-2013.

Burrows, J., Hölzle, E., Goede, A., Visser, H., Fricke, W., 1995. SCIAMACHY—Scanning imaging absorption spectrometer for atmospheric chartography. Acta Astronaut. 35 (7), 445–451.

Burrows, J.P., Weber, M., Buchwitz, M., Rozanov, V., Ladstätter-Weißenmayer, A., Richter, A., DeBeek, R., Hoogen, R., Bramstedt, K., Eichmann, K.-U., et al., 1999. The global ozone monitoring experiment (GOME): Mission concept and first scientific results. J. Atmos. Sci. 56 (2), 151–175.

Cao, C., De Luccia, F.J., Xiong, X., Wolfe, R., Weng, F., 2014. Early on-orbit performance of the visible infrared imaging radiometer suite onboard the suomi national polar-orbiting partnership (S-NPP) satellite. IEEE Trans. Geosci. Remote Sens. 52 (2), 1142–1156. http://dx.doi.org/10.1109/TGRS.2013.2247768.

Dang, R., Yang, Y., Hu, X.-M., Wang, Z., Zhang, S., 2019. A review of techniques for diagnosing the atmospheric boundary layer height (ABLH) using aerosol lidar data. Remote Sens. 11 (13), 1590. http://dx.doi.org/10.3390/rs11131590.

de Foy, B., Schauer, J.J., 2022. An improved understanding of NOx emissions in South Asian megacities using TROPOMI NO2 retrievals. Environ. Res. Lett. 17 (2), 024006.

Di Giuseppe, F., Rémy, S., Pappenberger, F., Wetterhall, F., 2018. Using the Fire Weather Index (FWI) to improve the estimation of fire emissions from fire radiative power (FRP) observations. Atmos. Chem. Phys. 18 (8), 5359–5370. http://dx.doi.org/10.5194/acp-18-5359-2018, URL: https://acp.copernicus.org/articles/18/5359/2018/.

Draxler, R., Stunder, B., Rolph, G., Stein, A., Taylor, A., Zinn, S., Loughner, C., Crawford, A., 2022. HYSPLIT user's guide version 5.2. In: Air Resources Laboratory. National Oceanic and Atmospheric Administration, USA, URL: https://www.arl.noaa.gov/documents/reports/hysplit_user_guide.pdf.

Eskes, H., van Geffen, J., Boersma, F., Eichmann, K.-U., Apituley, A., Pedergnana, M., Sneep, M., Veefkind, J.P., Loyola, D., 2022. Sentinel-5 Precursor/TROPOMI Level 2 Product User Manual Nitrogendioxide. Tech. Rep. S5P-KNMI-L2-0021-MA, Koninklijk Nederlands Meteorologisch Instituut (KNMI), URL: https://sentinel.esa.int/documents/247904/2474726/Sentinel-5P-Level-2-Product-User-Manual-Nitrogen-Dioxide.pdf, Accessed on March 13, 2023.

Eskes, H., Sneep, J.M., Veefkind, P., Niemeijer, S., Zehner, C., 2021. S5P nitrogen dioxide v02. 03.01 intermediate reprocessing on the S5P-PAL system: Readme file.

Fan, H., Yang, X., Zhao, C., Yang, Y., Shen, Z., 2023. Spatio-temporal variation characteristics of global wildfires and their emissions. Atmos. Chem. Phys. Discuss. 1–34. http://dx.doi.org/10.5194/acp-23-7781-2023.

Fehr, T., 2016. Sentinel-5 Precursor Scientific Validation Implementation Plan, Vol. 1. European Space Agency, Zenodo, p. 280. http://dx.doi.org/10.5281/zenodo.165739.

Fioletov, V., McLinden, C.A., Griffin, D., Krotkov, N., Liu, F., Eskes, H., 2022. Quantifying urban, industrial, and background changes in $NO_2$ during the COVID-19 lockdown period based on TROPOMI satellite observations. Atmos. Chem. Phys. 22 (6), 4201–4236. http://dx.doi.org/10.5194/acp-22-4201-2022, URL: https://acp.copernicus.org/articles/22/4201/2022/.

Fishman, J., Crutzen, P.J., 1978. The origin of ozone in the troposphere. Nature 274 (5674), 855–858.

Frederick, B., Charap, S., Mueller, K.P., 2022. Responding To a Limited Russian Attack on NATO During the Ukraine War. RAND Corporation, Santa Monica, CA, http://dx.doi.org/10.7249/PEA2081-1.

Galytska, E., Danylevsky, V., Hommel, R., Burrows, J.P., 2018. Increased aerosol content in the atmosphere over Ukraine during summer 2010. Atmos. Meas. Tech. 11 (4), 2101–2118. http://dx.doi.org/10.5194/amt-11-2101-2018, URL: https://amt.copernicus.org/articles/11/2101/2018/.

Griffin, D., McLinden, C.A., Dammers, E., Adams, C., Stockwell, C.E., Warneke, C., Bourgeois, I., Peischl, J., Ryerson, T.B., Zarzana, K.J., Rowe, J.P., Volkamer, R., Knote, C., Kille, N., Koenig, T.K., Lee, C.F., Rollins, D., Rickly, P.S., Chen, J., Fehr, L., Bourassa, A., Degenstein, D., Hayden, K., Mihele, C., Wren, S.N., Liggio, J., Akingunola, A., Makar, P., 2021. Biomass burning nitrogen dioxide emissions derived from space with TROPOMI: methodology and validation. Atmos. Meas. Tech. 14 (12), 7929–7957. http://dx.doi.org/10.5194/amt-14-7929-2021, URL: https://amt.copernicus.org/articles/14/7929/2021/.

Hobbs, P.V., Radke, L.F., 1992. Airborne studies of the smoke from the Kuwait oil fires. Science 256 (5059), 987–991, URL: http://www.jstor.org/stable/2877118.

Jin, Y., Liu, Y., Lu, X., Chen, X., Shen, A., Wang, H., Cui, Y., Xu, Y., Li, S., Liu, J., Zhang, M., Ma, Y., Fan, Q., 2023. Measurement report: Assessing the impacts of emission uncertainty on aerosol optical properties and radiative forcing from biomass burning in peninsular Southeast Asia. EGUsphere 2023, 1–43. http://dx.doi.org/10.5194/egusphere-2023-1650, URL: https://egusphere.copernicus.org/preprints/2023/egusphere-2023-1650/.

Lange, K., Richter, A., Burrows, J.P., 2022a. Variability of nitrogen oxide emission fluxes and lifetimes estimated from Sentinel-5P TROPOMI observations. Atmos. Chem. Phys. 22 (4), 2745–2767. http://dx.doi.org/10.5194/acp-22-2745-2022, URL: https://acp.copernicus.org/articles/22/2745/2022/.

Lange, K., Richter, A., Schönhardt, A., Meier, A.C., Bösch, T., Seyler, A., Krause, K., Behrens, L.K., Wittrock, F., Merlaud, A., Tack, F., Fayt, C., Friedrich, M.M., Dimitropoulou, E., Van Roozendael, M., Kumar, V., Donner, S., Dörner, S., Lauster, B., Razi, M., Borger, C., Uhlmannsiek, K., Wagner, T., Ruhtz, T., Eskes, H., Bohn, B., Santana Diaz, D., Abuhassan, N., Schüttemeyer, D., Burrows, J.P., 2022b. Validation of Sentinel-5P TROPOMI tropospheric $NO_2$ products by comparison with $NO_2$ measurements from airborne imaging, ground-based stationary, and mobile car DOAS measurements during the S5P-VAL-DE-ruhr campaign. Atmospheric Meas. Tech. Discuss. 2022, 1–45. http://dx.doi.org/10.5194/amt-2022-264, URL: https://amt.copernicus.org/preprints/amt-2022-264/.

Lowenthal, D.H., Borys, R.D., Chow, J.C., Rogers, F., Shaw, G.E., 1992. Evidence for long-range transport of aerosol from the Kuwaiti oil fires to Hawaii. J. Geophys. Res.: Atmos. 97 (D13), 14573–14580. http://dx.doi.org/10.1029/92JD00934, URL: https://agupubs.onlinelibrary.wiley.com/doi/abs/10.1029/92JD00934.

Lyashenko, V., Onopchuk, I., Tymoshchuk, O., Hlebchuk, H., Zakharchuk, I., Skliiarenko, A., Stakhovskyi, O., Chyzhenko, M., Mikhieiev, I., Shmurak, A., Balabuk, V., Trofimova, I., Malytska, L., Krakovska, S., Palamarchuk, L., Gnatiuk, N., Shpytal, T., 2022. Ukraine. In: 2022 National Inventory Report (NIR). United Nations (UN) Climate Change, URL: https://unfccc.int/documents/476868.

Manisalidis, I., Stavropoulou, E., Stavropoulos, A., Bezirtzoglou, E., 2020. Environmental and health impacts of air pollution: a review. Front. Public Health 14. http://dx.doi.org/10.3389/fpubh.2020.00014.

Melas, D., Zerefos, C., Rapsomanikis, S., Tsangas, N., Alexandropoulou, A., 2000. The war in Kosovo. Environ. Sci. Pollut. Res. 7, 97–104. http://dx.doi.org/10.1065/espr2000.02.016.

Oreshchenko, A., Osadchyi, I., Savenets, M., Balabukh, V., 2020. Detection and monitoring of potentially dangerous fires on the territory of Ukraine using the data of satellite scanning. Visn. Nac. Acad. Nauk Ukr. http://dx.doi.org/10.15407/visn2020.11.033.

Rémy, S., Veira, A., Paugam, R., Sofiev, M., Kaiser, J.W., Marenco, F., Burton, S.P., Benedetti, A., Engelen, R.J., Ferrare, R., Hair, J.W., 2017. Two global data sets of daily fire emission injection heights since 2003. Atmos. Chem. Phys. 17 (4), 2921–2942. http://dx.doi.org/10.5194/acp-17-2921-2017, URL: https://acp.copernicus.org/articles/17/2921/2017/.

Reuveny, R., Mihalache-O'Keef, A.S., Li, Q., 2010. The effect of warfare on the environment. J. Peace Res. 47 (6), 749–761. http://dx.doi.org/10.1177/0022343310382069, arXiv:https://doi.org/10.1177/0022343310382069.

Savenets, M., 2021. Air pollution in Ukraine: a view from the Sentinel-5P satellite. Időjárás/Q. J. Hung. Meteorol. Serv. 125 (2), 271–290. http://dx.doi.org/10.28974/idojaras.2021.2.6.

Savenets, M., Dvoretska, I., Nadtochii, L., Zhemera, N., 2022. Comparison of TROPOMI NO2, CO, HCHO, and SO2 data against ground-level measurements in close proximity to large anthropogenic emission sources in the example of Ukraine. Meteorol. Appl. 29 (6), e2108.

Savenets, M., Osadchyi, V., Oreshchenko, A., 2020. Forest fires in April 2020 and the resulting changes of air quality in Ukraine. Visn. Nac. Akad. Nauk Ukr 5, 80–89. http://dx.doi.org/10.15407/visn2020.05.080.

Schroeder, W., Giglio, L., 2018. NASA VIIRS Land Science Investigator Processing System (SIPS) Visible Infrared Imaging Radiometer Suite (VIIRS) 375 m & 750 m Active Fire Products: Product User's Guide Version 1.4. NASA, Washington, DC, USA, URL: https://viirsland.gsfc.nasa.gov/PDF/VIIRS_activefire_User_Guide.pdf.

Schroeder, W., Oliva, P., Giglio, L., Csiszar, I.A., 2014. The new VIIRS 375 m active fire detection data product: Algorithm description and initial assessment. Remote Sens. Environ. 143, 85–96. http://dx.doi.org/10.1016/j.rse.2013.12.008, URL: https://www.sciencedirect.com/science/article/pii/S0034425713004483.

Stein, A., Draxler, R.R., Rolph, G.D., Stunder, B.J., Cohen, M., Ngan, F., 2015. NOAA's HYSPLIT atmospheric transport and dispersion modeling system. Bull. Am. Meteorol. Soc. 96 (12), 2059–2077.

Tack, F., Merlaud, A., Iordache, M.-D., Pinardi, G., Dimitropoulou, E., Eskes, H., Bomans, B., Veefkind, P., Van Roozendael, M., 2021. Assessment of the TROPOMI tropospheric $NO_2$ product based on airborne APEX observations. Atmos. Meas. Tech. 14 (1), 615–646. http://dx.doi.org/10.5194/amt-14-615-2021, URL: https://amt.copernicus.org/articles/14/615/2021/.

UNDPPA, HD, 2019. Digital technologies and mediation in armed conflict. URL: https://peacemaker.un.org/sites/peacemaker.un.org/files/DigitalToolkitReport.pdf.

UNEP, 2022. The environmental impact of the conflict in Ukraine: A preliminary review. URL: https://wedocs.unep.org/20.500.11822/40746.

van Geffen, J., Boersma, K.F., Eskes, H., Sneep, M., ter Linden, M., Zara, M., Veefkind, J.P., 2020. S5P TROPOMI NO2 slant column retrieval: method, stability, uncertainties and comparisons with OMI. Atmos. Meas. Tech. 13 (3), 1315–1335. http://dx.doi.org/10.5194/amt-13-1315-2020, URL: https://amt.copernicus.org/articles/13/1315/2020/.

Vasyliuk, O., Nekrasova, O., Shyriaieva, D., Kolomytsev, G., 2015. A review of major impact factors of hostilities influencing biodiversity in the eastern Ukraine (modeled on selected animal species). Vestnik Zool. 49 (2), 145.

Veefkind, J.P., Aben, I., McMullan, K., Förster, H., De Vries, J., Otter, G., Claas, J., Eskes, H., De Haan, J., Kleipool, Q., et al., 2012. TROPOMI on the ESA Sentinel-5 Precursor: A GMES mission for global observations of the atmospheric composition for climate, air quality and ozone layer applications. Remote Sens. Environ. 120, 70–83.

Vukmirović, Z.B., Unkašević, M., Lazić, L., Tošić, I., 2001. Regional air pollution caused by a simultaneous destruction of major industrial sources in a war zone. The case of April Serbia in 1999. Atmos. Environ. 35 (15), 2773–2782. http://dx.doi.org/10.1016/S1352-2310(00)00530-6, URL: https://www.sciencedirect.com/science/article/pii/S1352231000005306.

Wieczorek, B., 2023. Air pollution patterns mapping of SO2, NO2, and CO derived from TROPOMI over central-east Europe. Remote Sens. 15 (6), http://dx.doi.org/10.3390/rs15061565, URL: https://www.mdpi.com/2072-4292/15/6/1565.

Zhang, C., Hu, Q., Su, W., Xing, C., Liu, C., 2023. Satellite spectroscopy reveals the atmospheric consequences of the 2022 Russia-Ukraine war. Sci. Total Environ. 869, 161759. http://dx.doi.org/10.1016/j.scitotenv.2023.161759, URL: https://www.sciencedirect.com/science/article/pii/S0048969723003741.

Zhang, C., Shulga, V., Milinevsky, G., Danylevsky, V., Yukhymchuk, Y., Kyslyi, V., Syniavsky, I., Sosonkin, M., Goloub, P., Turos, O., et al., 2022. Spring 2020 atmospheric aerosol contamination over Kyiv City. Atmosphere 13 (5), 687. http://dx.doi.org/10.3390/atmos13050687.